International Journal of Remote Sensing, 2014
Vol. 35, No. 3, 927–948, http://dx.doi.org/10.1080/01431161.2013.873833

Taylor & Francis
Taylor & Francis Group

DEM generation from lidar data in wooded mountain areas by cross-section-plane analysis

Haiyan Guan[a], Jonathan Li[a,b]*, Yongtao Yu[b], Liang Zhong[c], and Zheng Ji[d]

[a]*Department of Geography & Environmental Management, University of Waterloo, Waterloo, ON, Canada N2L 3G1;* [b]*Key Laboratory of Underwater Acoustic Communication and Marine Information Technology, School of Information Science and Engineering, Xiamen University, Xiamen, Fujian 361005, China;* [c]*Changjiang Spatial Information Technology Engineering Company, Changjiang Institute of Survey Planning Design and Research, Wuhan, Hubei 430010, China;* [d]*School of Remote Sensing Information & Engineering, Wuhan University, Wuhan, Hubei 430079, China*

(*Received 20 September 2012; accepted 3 November 2013*)

Ground filtering for airborne lidar data is a challenging task for the generation of digital terrain models (DTMs) in wooded mountain areas. To solve this problem, this article, based on cross-section-plane (CSP) analysis, presents a CSP-based stepwise filtering strategy that can automatically separate terrain from non-terrain points. The filtering strategy consists of four main computing steps: (a) 'split' – the raw lidar data are partitioned into 3D cells, in each of which multi-directional CSPs are generated at multiple directions; (b) 'filter' – the potential terrain points are selected for each CSP according to lidar data characteristics, such as multi-returns, intensity, and height; (c) 'detect' – the initial terrain points are detected for each CSP by exploring distances and slopes between nearby points; and (d) 'adjust-and-refine' – the terrain points are extracted from all initial terrain points of all CSPs by a merging-or-intersecting strategy and a five-point refinement. The extensive experiments using three lidar data sets demonstrated that the CSP-based stepwise filtering method is capable of producing reliable DTMs in densely forested mountain areas.

1. Introduction

Compared to traditional techniques, such as field surveys and photogrammetry, light detection and ranging (lidar) has proved an effective method for rapidly generating digital terrain models (DTMs), often termed 'ground filtering' (Pfeifer et al. 1999; Pfeifer and Mandlburger 2008; Meng, Currit, and Zhao 2010). However, separating terrain from non-terrain points in a lidar point cloud is a challenging task, especially in a wooded mountainous area with complex terrain variations (Liu 2008; Mongus and Zalik 2012). Related work about filtering algorithms of lidar point clouds can be found in the literature (e.g. Sithole and Vosselman 2004; Pfeifer and Mandlburger 2008; Li and Guan 2010; Meng, Currit, and Zhao 2010; Briese 2010; Bartels and Wei 2010). Several important issues need to be considered in a filtering process, including input data, iterative characteristics, lidar penetration, pre-processing steps, neighbourhood types, and other key factors. In the following paragraphs, we roughly classify the existing filtering algorithms into several categories based on the characteristics of filtering algorithms.

*Corresponding author. Email: junli@uwaterloo.ca

Assuming that terrain is a continuous or piecewise continuous surface, surface-based methods select seeds from point clouds to calculate an initial parametric surface, and iteratively search new ground points only if those points meet certain data-derived threshold parameters (e.g. the difference in elevation, slope) (Kraus and Pfeifer 1998; Axelsson 2000; Pfeifer, Stadler, and Briese 2001; Sohn and Dowman 2002). However, these surface-based algorithms require considerable computation times (Seo and O'Hara 2008). As morphological filters provide a quantitative description of a geometrical structure based on structuring elements, they are sensitive to the size of the morphological structuring elements (Wack and Wimmer 2002; Kilian, Haala, and Englich 1996; Zhang et al. 2003; Zhang and Whitman 2005; Chen et al. 2007; Pfeifer and Mandlburger 2008). Although morphological filters are conceptually simple and can be easily implemented, the interpolation of point clouds leads to a significant loss of information and causes errors in the results (Axelsson 1999). Slope-based methods perform a filtering operation using slope or difference in elevation between two points. If the slope or difference in elevation exceeds a certain threshold, the higher point is classified as an object over the ground surface (Vosselman 2000; Vosselman and Maas 2001; Sithole 2001; Roggero 2001; Shao and Chen 2008). However, these slope-based filters are unsuitable for steep terrain, and are especially unreliable in the cases of steep, forested areas (Liu 2008).

A set of segmentation-based and clustering methods, popular techniques in land-use and land-cover classification, have been gaining popularity in the filtering of lidar data (Nardinocchi, Forlani, and Zingaretti 2003; Sithole and Vosselman 2005; Tovari and Pfeifer 2005; Filin and Pfeifer 2006). These methods segment point clouds into a number of segments with a local neighbourhood analysis and subsequently classify the segments by different classification strategies (e.g. region-growing) with respect to similarity measures, such as differences in elevation, normal vector similarity, and distances of points to a plane. The segmentation-based filtering methods are less affected by noise because they work on rasterized data and deal with larger entities (i.e. they are not based on individual points or pixels). However, they are usually carried out on fairly flat ground surfaces, and their accuracies decline with increasingly steep terrain (Pfeifer and Briese 2007; Pfeifer and Mandlburger 2008; Liu 2008). Recently, machine-learning approaches such as the support vector machine (Lodha et al. 2006) and conditional random field (Lu et al. 2009) have been applied to lidar point clouds. Although these machine-learning methods might obtain promising filtering results, the selection of training samples is one of the critical issues in terrain filtering. In order to select training sets that must be representative of the whole lidar data, human interactions are required, resulting in unreliable classification results.

In recent years, statistical filtering algorithms have been explored, such as skewness balancing (Bartels and Wei 2010), and a predictive Kalman filter and Bayesian framework (Bretar and Chehata 2010). The skewness balance-based filter is an unsupervised, parameter-free classification algorithm for object and ground point separation in airborne lidar data (Bartels and Wei 2010). However, prior to the use of skewness balancing, some conditions such as the minimum number of ground points have to be satisfied. In addition, the skewness balance-based filter is unable to filter out attached objects such as buildings on slopes, bridges, and ramps. The predictive Kalman filter and Bayesian framework is unable to preserve crests and flanks in mountainous landscapes. Moreover, in the case of dense vegetation, the filtered terrain is locally smoothed.

Because most of the aforementioned methods involve iterations, they are computationally intensive and time consuming, which causes serious problems for processing a massive volume of lidar data. Thus, a scan-line technique was proposed to identify ground points by elevation or slope profiles (Sithole 2001; Meng et al. 2009). Shan and Sampath

(2005) filtered out ground points by applying a scan-line-based one-dimensional (1D) and bi-directional labelling filter to lidar data in urban areas. Meng et al. (2009) extended the bi-directional filter to a multi-directional filtering strategy. Although, these algorithms delivered unreliable filtering results when handling complex terrain surfaces such as steep slopes, super building structures, or break-lines, the 2D profile-based algorithms can deal with lidar data efficiently.

Currently, it is challenging to extract ground points from lidar points in mountainous areas covered with dense vegetation because of fewer lidar points hitting the surface of the Earth or because of large height differences over small horizontal distances (Kobler et al. 2007). Raber et al. (2002) created digital elevation models (DEMs) using an adaptive lidar vegetation point removal process based on multi-return lidar characteristics. Hyyppä et al. (2000) suggested that the accuracy of DTMs is related not only to flight plans and misalignment but also to terrain slopes and vegetation density. Therefore, according to implicit data characteristics (e.g. point density, multi-return) and terrain features to be processed, knowledge-based filtering strategies have been exploited to create rules from training data sets (Brenner 2000; Zhou and Troy 2008). Apart from geometric information, information from the same sensor or other information from sensors can be employed to improve automation and filtering accuracy (Pfeifer and Mandlburger 2008). Through statistical analysis, features of investigated areas are highlighted to automatically determine filtering thresholds.

To generate DTMs in steep forested areas, this article presents a robust stepwise filtering algorithm that first analyses lidar data by multi-directional CSPs that are similar to 2D profiles for efficiently processing lidar data. With the CSPs, we then take into account lidar data characteristics, such as intensity, height, and multi-returns, to remove unwanted non-terrain points, followed by a slope-based scheme for identifying terrain points. A post-process is finally necessary to refine the identified terrain points. The remainder of the article is organized as follows. The next section provides the concept behind our CSP-based algorithm. Then, our filtering algorithm will be presented in Section 3, addressed by split, filter, detect, and adjust-and-refine. This is followed by a presentation and discussion of the results obtained from three lidar data sets in Section 4. Finally, Section 5 concludes the article and suggests future research directions.

2. CSP

A CSP is a useful way to observe and analyse inner structures of 3D spatial objects. The difficulty or complexity of a 3D object can be decreased by slicing it into a number of 2D CSPs at multiple directions. We can analyse and synthesize information from 2D CSPs to achieve a representation of a 3D complex object. Habib, Chang, and Lee (2009) checked all possible directions to detect occluded points for the classification of lidar data. Thus, usage of CSPs makes it possible to view geometric characteristics within complex unstructured 3D raw point clouds in detail.

The output of a lidar system is a collection of geometrically irregular or unstructured 3D raw point clouds. The term ‘unstructured’ in this context means that spatial relationships between points are not clearly presented. A large quantity of point clouds leads to interpolation difficulties in manual interaction and data inspection. Therefore, profiling a whole set of lidar data into a number of sections with the certain widths or lengths at given directions is an effective way for quality inspection. Figure 1(*a*) shows a range image of a mountain area, while Figures 1(*b*)–(*e*) show four CSPs observed from directions A, B, C, and D for the bold blue dashed lines shown in Figure 1(*a*). These CSPs

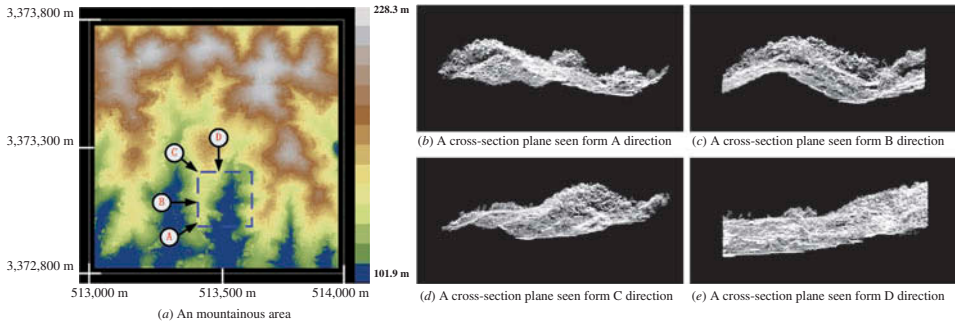

Figure 1. Range image of a mountain area (*a*), and CSPs from directions A (*b*), B (*c*), C (*d*), and D (*e*).

show detailed information about local topographic variations and relief of the mountain area, indicating that the lidar information observed from multi-directional CSPs can enhance the possibilities of separating terrain from non-terrain points.

3. CSP-based method

In this article, the objective is to analyse a large quantity of 3D point clouds via a 2D CSP perspective and identify terrain points in steep forested areas. The proposed filtering method can be seen as a stepwise procedure for interpreting lidar data. The method includes the following four main steps.

(1) Split: Partition the raw lidar data into 3D cells and generate multi-directional CSPs for each cell at multiple directions.
(2) Filter: Select potential terrain points for each CSP regarding lidar data characteristics, such as multi-returns, intensity, and height.
(3) Detect: Detect the initial terrain points for each CSP by exploring distances and slopes between nearby points.
(4) Adjust-and-Refine: Merge or intersect all initial terrain points of all CSPs for each cell, and apply a five-point method to the merged or intersected terrain points for the improvement of filtering quality.

The rest of this section describes our method step by step. Sections 3.1–3.4 detail the generation of terrain points via four main steps: split, filter, detect, and merge/intersect-and-refine, as shown in Figure 2.

3.1. Split

It is critical to deal with a large-scale lidar data set and identify interesting objects automatically. To manage such data efficiently, we split the whole lidar point data set P into 3D cells. After loading a large volume of point cloud P, we calculate a bounding box, the maximum and minimum along *X*-, *Y*-, and *Z*-axes (X_{max}, X_{min}; Y_{max}, Y_{min}; Z_{max}, Z_{min}), according to all points in P. The size of the cells is user-defined

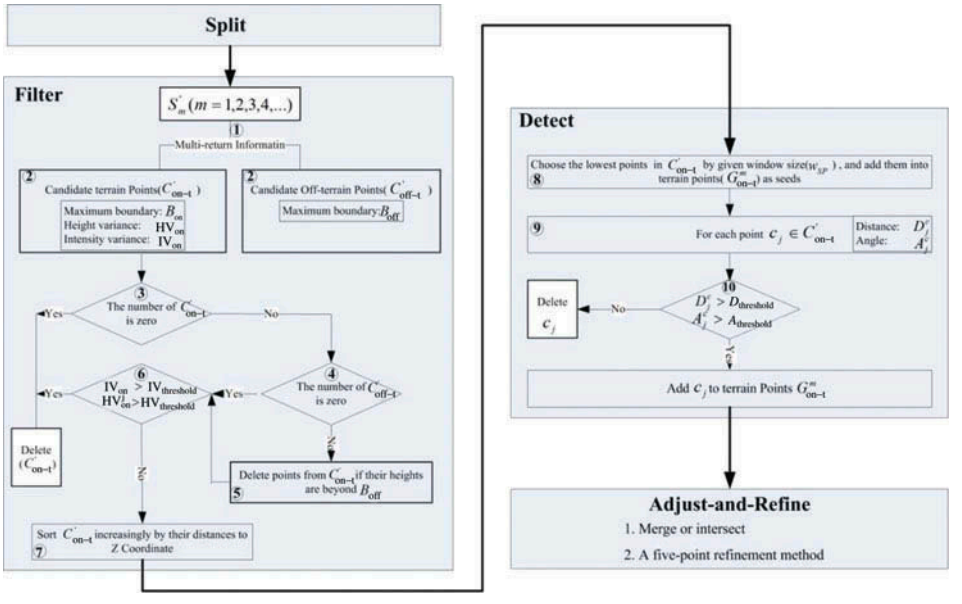

Figure 2. Flow chart of our CSP-based stepwise filtering algorithm for separating terrain from non-terrain points.

(e.g. w_{length}, w_{width}, w_{height}); and the number of the cells along X-, Y-, Z-axes (N_x,N_y,N_z) can be defined as

$$\begin{cases} N_x = \text{INT}((X_{\max} - X_{\min})/w_{\text{length}}) \\ N_y = \text{INT}((Y_{\max} - Y_{\min})/w_{\text{width}}) \\ N_z = \text{NT}((Z_{\max} - Z_{\min})/w_{\text{height}}) \end{cases}. \tag{1}$$

Based on the assumption that the lowest point in a local neighbourhood has a higher possibility of being a terrain point, we do not partition the lidar data in the Z-axis, that is, $w_{\text{height}} = (Z_{\max} - Z_{\min})$ and $N_z = 1$. We define $w_{\text{length}} = w_{\text{width}} = w$ to obtain uniform cells $V_{i,j}(i = 0, 1, 2, ..., N_x; j = 0, 1, 2, ..., N_y)$ along the X- and Y-axes.

Assume that we project all points of each cell $V_{i,j}$ onto four cardinal directions ($\varphi = 0°$, 45º, 90º, and 135º, 0º $\leq \varphi < 180°$), respectively. Correspondingly, we can obtain four CSPs, $S_m^{'}(m = 1, 2, 3, 4)$, for each cell, as shown in Figure 3. We find that CSPs at different directions exhibit different representations of the same 3D complex object. For example, by a simple slope-based filtering scheme, we can successfully identify more true terrain points on $S_1^{'}$ than those on $S_2^{'}$ because a mix of tree and terrain points on $S_2^{'}$ are often treated as an upward slope by most filtering methods.

3.2. Filter

For each of the CSP data, $S_m^{'}$, we attempt to filter out non-terrain points using lidar data characteristics, such as multi-returns, intensity, and height variances. Although last-returns of a pulse are not always reflected from the ground, first- and middle-returns of the pulse are mainly reflected from vegetation (see Figure 4). Therefore, we remove first- and middle-returns from lidar data and just retain single-returns and last-returns. Also, lidar

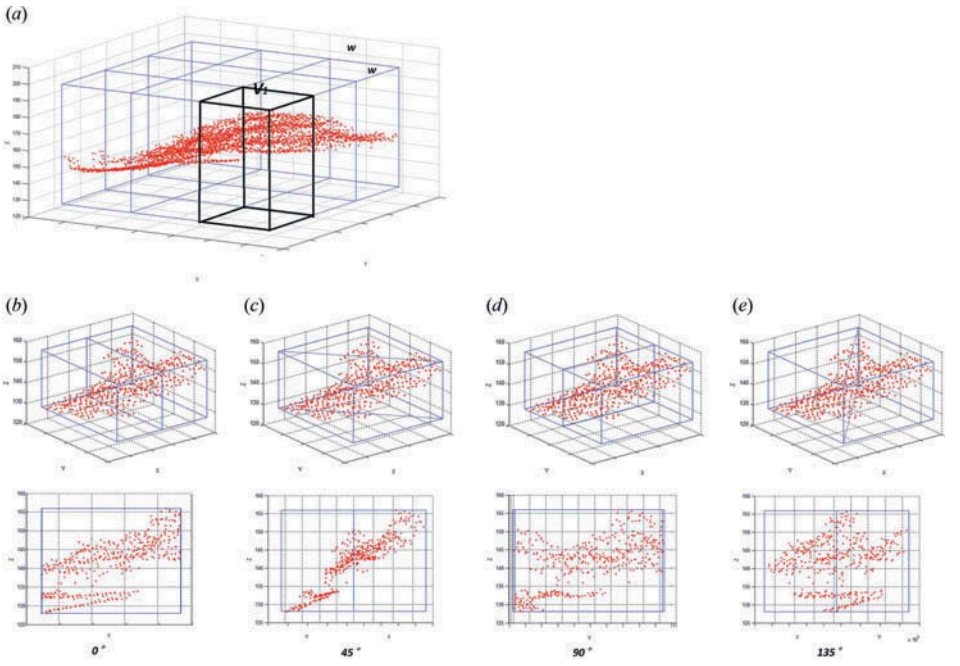

Figure 3. Illumination of four CSPs of each cell: (*a*) splitting lidar data, (*b*) a CSP S_1' at 0°, (*c*) S_2' at 45°, (*d*) S_3' at 90°, and (*e*) S_4' at 135°.

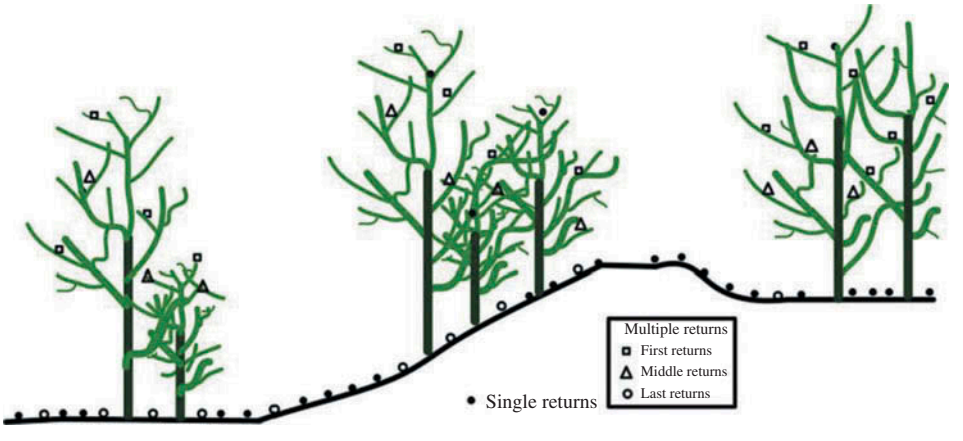

Figure 4. Description of discrete multiple returns.

intensity information can be used to extract planimetric features and serve as ancillary input for lidar data processing after radiometric calibration because intensity is related to the reflective properties of targets as well as the light used (Donoghue et al. 2007). For example, in the range of the near-infrared spectrum (~900–1500 nm) vegetation and soil have distinct reflective characteristics in densely wooded mountain areas. Height variances, the height differences between lidar points and the mean point, are also used to

discriminate terrain and non-terrain points. As Wang and Glenn (2009) have noted, comprehensive utilization of spatial and spectral information is better than using either alone. Therefore, we use multiple returns, intensity, and height variance to remove non-terrain points and reduce processing time to a certain extent.

As shown in Figure 2, the filter for each of the CSP data, $S_m^{'}$, is detailed as follows.

Step 1: A point v_i ($v_i \in P$, i = 1, 2, 3,…, I (I is the number of lidar points in P) is classified as $C_{\text{on-t}}^{'}$ (candidate terrain points) if it is single- or last- return; otherwise point v_i is labelled as $C_{\text{off-t}}^{'}$ (candidate non-terrain points) if it is first- or middle-return:

$$\forall v_i \begin{cases} \text{if}(v_i \text{ is single-/last-return}), & C_{\text{on-t}}^{'} \\ \text{else}, & C_{\text{off-t}}^{'} \end{cases}. \tag{2}$$

Step 2: Denote B_{off} and B_{on} as the maximum boundary of $C_{\text{off-t}}^{'}$ and $C_{\text{on-t}}^{'}$, respectively. According to Equation (3), we calculate height ($\text{HV}_{\text{on}}^{j}$) and intensity variances ($\text{IV}_{\text{on}}^{j}$) for each point c_j ($c_j \in C_{\text{on}-\text{t}}^{'}$, j = 1, 2, 3,…, J, J is the number of lidar points in $C_{\text{on-t}}^{'}$) in the data set $C_{\text{on-t}}^{'}$, where, H_j and I_j are the values of elevation and intensity for the point c_j, respectively.

$$\begin{cases} \text{HV}_{\text{on}}^{j} = \dfrac{\sum (H_j - \bar{H}_{\text{on}})^2}{J} & \bar{H}_{\text{on}} = \dfrac{\sum_{j}^{m} H_j}{J} \\ \text{IV}_{\text{on}}^{j} = \dfrac{\sum (I_j - \bar{I}_{\text{on}})^2}{J} & \bar{I}_{\text{on}} = \dfrac{\sum_{j}^{m} I_j}{J} \end{cases}. \tag{3}$$

Step 3: If the number of $C_{\text{on-t}}^{'}$ (J = 0) is larger than zero, proceed to the next step; otherwise, delete $C_{\text{on-t}}^{'}$.

Step 4: If the number of $C_{\text{off-t}}^{'}$ is not equal to zero, proceed to Step 5; otherwise, move to Step 6.

Step 5: Points $c_j \in C_{\text{on-t}}^{'}$, whose heights range beyond B_{off}, are removed, and then proceed to the next step.

Step 6: Points $c_j \in C_{\text{on-t}}^{'}$, whose height variances $\text{HV}_{\text{on}}^{j}$ and intensity variance $\text{IV}_{\text{on}}^{j}$ are both larger than the height variance threshold $\text{HV}_{\text{threshold}}$ and the intensity variance threshold $\text{IV}_{\text{threshold}}$, are removed. This means that there are too many points reflecting from the tree canopy, not from the ground because of dense vegetation. Otherwise, move into the next step. The determination of $\text{HV}_{\text{threshold}}$ and $\text{IV}_{\text{threshold}}$ is automatic and dependent on the lidar points. In the article, we assume that the lowest points are on the terrain, and randomly select couples of the lowest points from the investigated cell and its neighbour cells to form an initial terrain data set. $\text{HV}_{\text{threshold}}$ and $\text{IV}_{\text{threshold}}$ are calculated from the initial terrain points.

Step 7: Points $c_j \in C_{\text{on-t}}^{'}$ are sorted by their distances to the Z-coordinate, and are rearranged to a scan line to move into the next detect step.

3.3. *Detect*

The points left in $C_{\text{on-t}}^{'}$ for each $S_m^{'}$ are further processed to separate terrain from non-terrain points (see Figure 2). The algorithm assumes that the lowest point in a neighbourhood is a ground point. The detect procedure is detailed as follows.

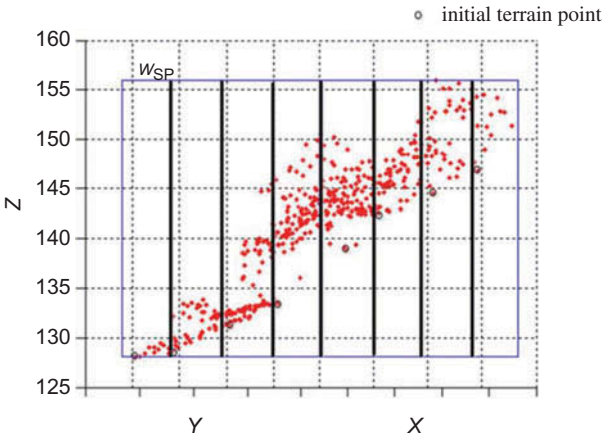

Figure 5. Segmentation of a CSP with a given segment width w_{SP}, and the lowest points in each segment are picked up as initial terrain points.

Step 8: We segment the scan line with a given segment width w_{SP}, as can be seen in Figure 5. The segment width w_{SP} is estimated by using the covered length of the CSP, the number of points, and the number of user-defined minimum points in each segment:

$$w_{SP} = \frac{V_l}{I} U_{N\ of\ min}, \tag{4}$$

where I is the number of terrain points for each cell, which is related to the cell size (w) and point density, V_l is the covered length of a CSP, and $U_{N\ of\ min}$ is the number of user-defined minimum points in a segment cell. For example, if w is 10 m, the point density is 4 points/m^2, and V_l at 145° direction is $\sqrt{2}w$, w_{SP} is about 0.35 m if we attempt to keep 10 points in each grid cell.

After segmenting the scan line, the lowest points in each segment, as shown in Figure 5, are picked up as seed points to create an initial terrain point data set $G^m_{on\text{-}t}$ (g_l, $g_l \in G^m_{on\text{-}t}$, $l = 1, 2, 3,\ldots, L$, L is the number of lidar points in $G^m_{on\text{-}t}$), and removed from $C'_{on\text{-}t}$. The algorithm iteratively classifies terrain points via a triangulated surface model.

Step 9: For each point $c_j \in C'_{on\text{-}t}$, the minimum distance D^c_j to the nearest triangle node and the slope A^c_j are calculated, respectively, as shown in Figure 6.

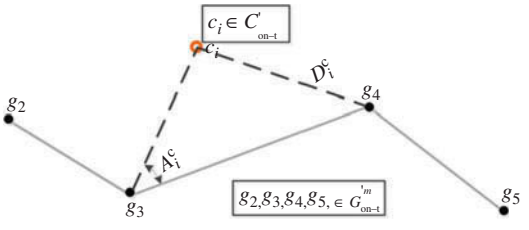

Figure 6. Illumination of terrain point collection.

Step 10: If a point c_j meets the distance difference and slope criteria with two nearest points $g_l \in G_{\text{on-t}}$, that is $D_j^c > D_{\text{threshold}}$ and $A_j^c > A_{\text{threshold}}$, this point will be added to $G_{\text{on-t}}$. The process is iterative until no point meeting these criteria remains.

3.4. *Adjust-and-refine*

Having dealt with multi-directional CSPs $S_m^{'}(m = 1, 2, 3, 4, ...)$ for a 3D cell, we achieve the final filtering results ($G_{\text{on-t}}$) by merging or intersecting all multiple filtered terrain point data sets

$$G_{\text{on-t}}^m(m = 1, 2, 3, 4, ...) \text{ as } G_{\text{on-t}} = \begin{cases} G_{\text{on-t}}^1 \cup G_{\text{on-t}}^2 \cup G_{\text{on-t}}^3 \cup G_{\text{on-t}}^4 \cup ... \\ \text{or} \\ G_{\text{on-t}}^1 \cap G_{\text{on-t}}^2 \cap G_{\text{on-t}}^3 \cap G_{\text{on-t}}^4 \cap ... \end{cases}$$

In practice, whether the merging or intersecting strategy is applied to the filtered results is dependent on the terrain features and the point density. If the investigated terrain is continuously undulating (i.e. few break-lines exist), the intersecting strategy is preferred as it keeps the terrain relatively continuous and smooth. Otherwise, the merging strategy should be used since several different directions of CSPs can retain abruptly undulating features. If the point density is high, the intersecting strategy is primarily considered to generate DEMs because there are enough points to represent the detailed terrain characteristics.

To further remove non-terrain points from the filtered results, a five-point refinement method is used regarding the spatial relation of an investigated point and its neighbours (see Figure 7) by the following rules.

- If Point P is below Line Segment P_2P_4, Point P is retained as a terrain point (see Figure 7(*a*)), otherwise, proceed to the next step;
- If the horizontal slope α1 of Line Segment P_1P_2 is opposed to the horizontal slope α_3 of Line Segment P_4P_5, Point P is retained as a mountainous ridge point, as Figure 7(*b*) shows; otherwise, proceed to the next step;
- If both of the slope differences $\Delta_1(|\alpha_2 - \alpha_1|)$ and $\Delta_2(|\alpha_2 - \alpha_3|)$ are smaller than the slope threshold Δα (according to the experiments, Δα is generally set as 10–15°, less than $A_{\text{threshold}}$), Point P is retained as a terrain point; otherwise, it is removed from the terrain points.

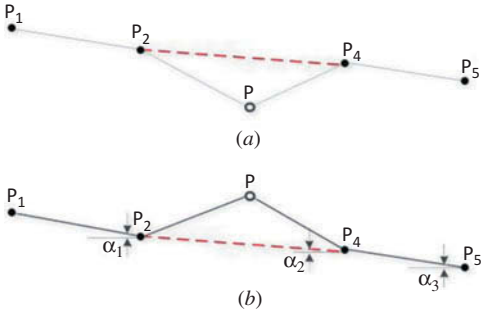

Figure 7. Five-point method for the refinement of the filtered results.

Through the five-point refinement method, the misclassified terrain points are eliminated.

4. Results and discussion

4.1. Data sets

Three data sets have been used in this article to assess the proposed CSP-based stepwise filtering method. The first two sets were collected in the multi-return mode by a Leica ALS50-II mounted on a helicopter. Data sets I and II were acquired in Taishan, Shandong, eastern China, in October 2004 and in Sichuan, southwestern China, in May 2008, respectively. Although both of them are wooded mountain areas with dense vegetation, Test-site I is relatively smooth compared to Test-site II. Thus, Test-site I is used to test whether the proposed filtering algorithm is robust enough to deal with wooded mountain areas. For the accuracy assessment, error computation for DTM generation is completed by comparing with the well-known Terrasoild® point cloud processing software suite. To extend the test to denser vegetation and more complex terrain areas, Test-site II is used to validate the proposed method. The last data set comes from the International society for Photogrammetry and Remote Sensing (ISPRS) Commission III/WG3, which provides eight study sites with both first and last returns in urban and rural environments. We select these 15 sites to further test our filtering algorithm and compare the algorithm with other filtering methods evaluated by ISPRS. All processing is implemented by VC++ in Microsoft Visual Studio 2005®.

4.2. Test-site I

Figure 8(*a*) shows a shaded relief map of a digital surface model (DSM) of Test-site I. The flying height ranges from 1100 to 1300 m above the ground, with a ground speed of about 100 km h^{-1} and a laser divergence of 0.22 mrad. The specifications of the instrument state that the vertical measurement accuracy is ±15 cm, and the horizontal accuracy is ±35 cm in either direction for the given flying height, that the field of view (FOV) is 45°, and that currently available systems offer pulse repetition frequency values between 90 kHz and 150 kHz with a density of about 1 point/m^2. We select a representative mountainous area for testing. The white square shown in Figure 8(*a*) depicts an undulating terrain with an area of 1 km^2. Figure 8(*a*) depicts a close view of the test site. There are a total of 1,224,513 points with the ground elevation ranging from 101.9 m to 228.33 m.

4.2.1. Sensitivity analysis

Table 1 lists all parameters and their thresholds used in this work. Among them, the thresholds of intensity and height variance in the filter step, $HV_{threshold}$ and $IV_{threshold}$, are calculated automatically according to the characteristics of the investigated ground features. In this work, one of the key parameters, w, is used to control cell size. The thresholds D and A are two other important criteria for DEM generation in the detect step. Thus, we conducted a series of experiments to test how these three parameters influence the accuracy of a lidar-derived DEM using 15 sets of thresholds.

The selected thresholds are shown in Table 2. To assess the filter performance, terrain and non-terrain points are manually classified with the help of the Terrasolid® software

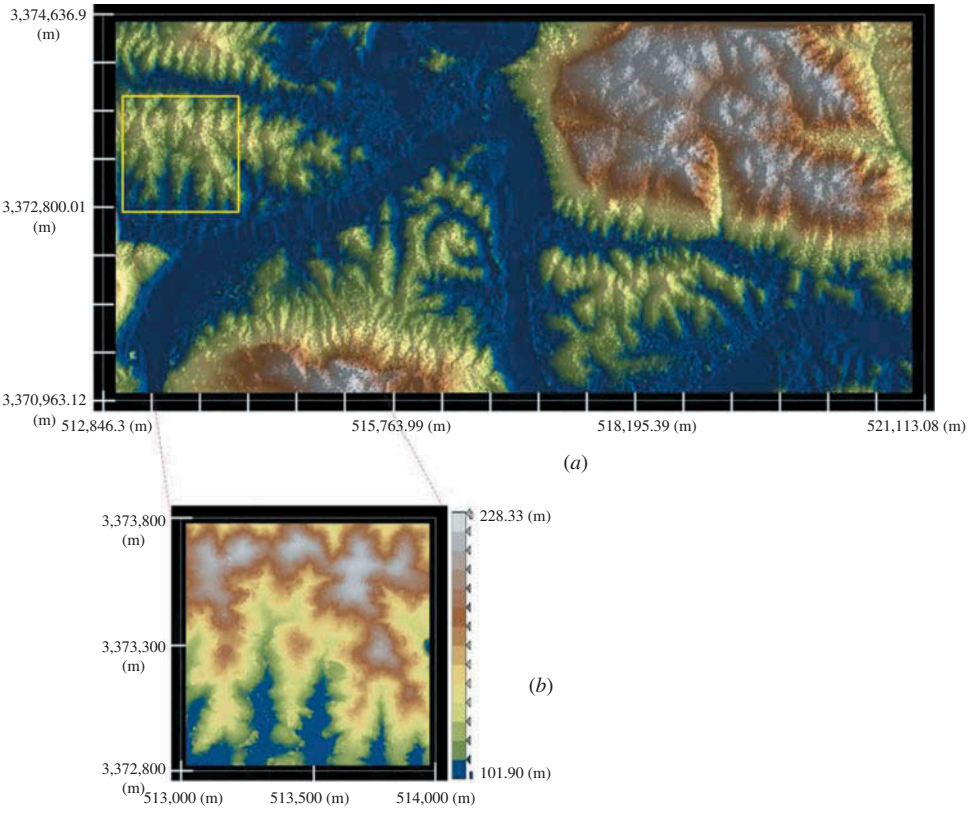

Figure 8. Test-site I: a mountain area with a smoother terrain.

Table 1. Parameters and their thresholds used in the article.

Parameters			
No.	Name	Explanation	Threshold value
1	w	The cell size for splitting	***To be investigated***
2	HV	Height variance in the filter step	$HV_{threshold}$ (Automatic)
3	IV	Intensity variance in the filter step	$IV_{threshold}$ (Automatic)
4	w_{SP}	The segment size	Depending on point density and w
5	D	Distance criterion in the detect step	$D_{threshold}$ ***(to be investigated)***
6	A	Slope criterion in the detect step	$A_{threshold}$ ***(to be investigated)***
7	$\Delta\alpha$	Slope difference criterion in the adjust-and-refine step	Less than $A_{threshold}$, and 5~10

suite as the reference data set. As Kobler et al. (2007) and Silthole and Vosselman (2004) suggested, the manual filtering could be seen as the best possible classification method given no additional information because human eyes can observe filtering errors easily. Therefore, this method is suggested for validation and comparison of filtering algorithms. In this article, we use a kappa coefficient as a measure of overall agreement of an error

Table 2. Parameters and kappa coefficients of the CSP method.

Test no.	Cell size (m)	$D_{threshold}$ (m)	$A_{threshold}$ (deg)	Kappa
1	10.0	0.5	30	0.8413
2	10.0	0.5	45	0.8398
3	10.0	0.5	60	0.8402
4	10.0	1.0	30	0.8507
5	10.0	1.0	45	0.8471
6	10.0	1.0	60	0.8427
7	10.0	1.5	30	0.8135
8	10.0	1.5	45	0.8140
9	10.0	1.5	60	0.8077
10	15.0	0.5	30	0.7820
11	15.0	1.0	30	0.8134
12	15.0	1.5	30	0.7865
13	20.0	0.5	30	0.7628
14	20.0	1.0	30	0.6856
15	20.0	1.5	30	0.7139

matrix. The kappa coefficient, introduced to the remote-sensing community in the early 1980s (Congalton and Mead 1983), has been recommended by Rosenfield and Fitzpatrick-Lins (1986) as a standard of accuracy assessment. Unlike the overall accuracy, the ratio of the sum of diagonal values to the total number of cell counts in the error matrix means the kappa coefficient also takes non-diagonal elements into account.

Table 2 shows that the kappa coefficients vary only a little from Tests 1 to 3, Tests 4 to 6, and Tests 7 to 9 with the fixed cell size w and distance difference threshold $D_{threshold}$. Figure 9(*a*) shows that the slope parameters are insensitive to the results. Notice that the distance difference parameters would be more sensitive than the slope parameters. This is due to the distance equations of points to a plane actually constraining the slopes. In practice, we can find that the $A_{threshold}$ of 30° is suitable for many terrain types. Figure 9(*b*) shows that the kappa coefficients increase with the increase of $D_{threshold}$ from 0.5 m to 1.0 m, while they subsequently decrease with the $D_{threshold}$ changed from 1.0 m to 1.5 m. Thus, $D_{threshold}$ of 1.0 m is favourable for the test areas. Figure 9(*c*) shows the sensitivity of the cell size to the filtering results. Notice that the quality of DEM decreases as the cell size w increases. Figure 11 shows the shaded relief maps of DEMs with three different cell sizes: 10 m, 15 m, and 20 m.

We find that the smaller the cell size is, the more details the terrain features of the mountain area are retained (see Figure 10). Meanwhile, filtering errors are also increasing, especially non-terrain points misclassified as terrain points. Figure 10(*a*) shows that some detailed terrain features are smoothed when using a relatively larger cell size (e.g. 20 m). However, as shown in Figure 10(*c*), there are a few errors in the relieved DEM when w = 10 m. Compared to these two examples, filtering results demonstrate that using the cell size of 15 m can retain terrain features, but also remove non-terrain points to the maximum extent. However, if a mountain area is covered by very dense vegetation, it is difficult to find terrain points. We then may have to enlarge the cell size to find points hitting on the ground. Figures 11(*a*) and (*b*) show a part of the filtered results of a CSP and a close view of the part identified by the black circle. As shown in Figure 11(*b*), the terrain is well maintained.

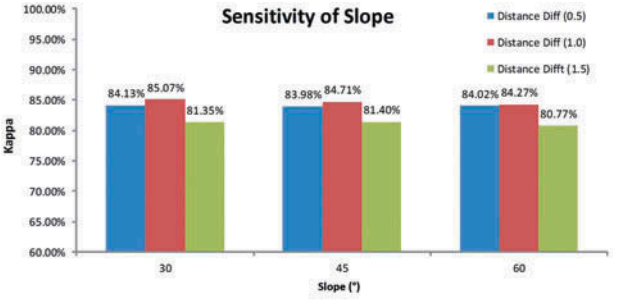

(*a*)

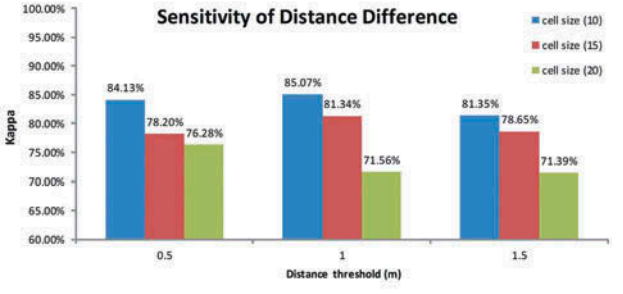

(*b*)

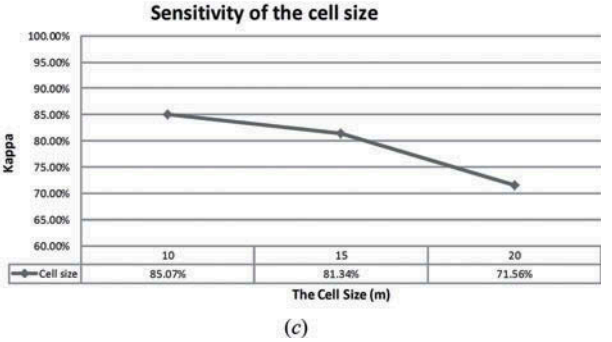

(*c*)

Figure 9. Error comparisons with three parameters: (*a*) a group of tests for sensitivity of the slope threshold; (*b*) a group of tests for sensitivity of the distance threshold; and (*c*) a group of tests for sensitivity of the cell size.

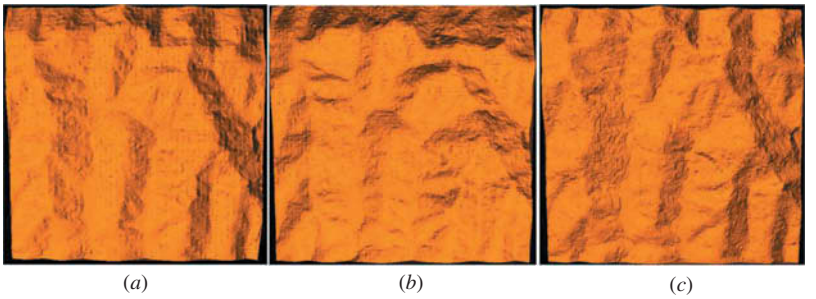

(*a*) (*b*) (*c*)

Figure 10. DEMs with different cell size: (*a*) 20 m; (*b*) 15 m; and (*c*) 10 m.

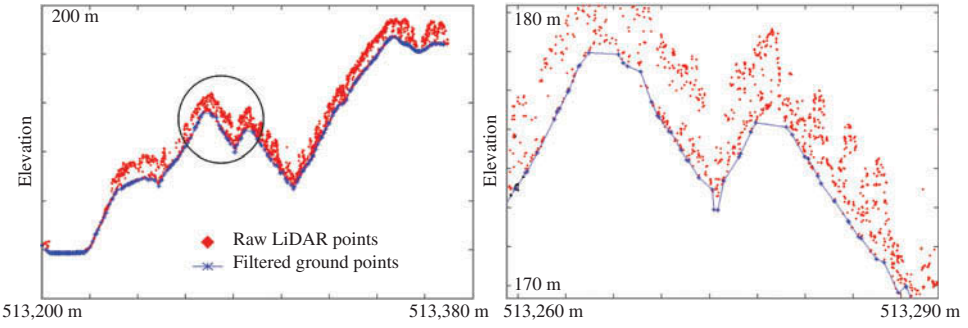

Figure 11. A close visual inspection from a profile: (*a*) the filtering results from a profile; and (*b*) a close visualization of the black circle in (*a*).

4.2.2. *Multiple features*

To evaluate contributions of lidar data features (e.g. multi-returns, height variance, and intensity information) on separating terrain from non-terrain points, we randomly select several small parts of Test-site I, as shown in Figure 12, to test whether these ancillary features can assist in the improvement of filtering accuracy. Table 3 shows the comparative results. In the filter step, each sample's non-terrain points, accounting for an average 15% of all total lidar points, are filtered out. Compared to the filtering results without the filter step, kappa coefficients for the filtering result with the filter step are increased obviously. This experiment therefore demonstrates that geometric and spectral information pertaining to lidar points can improve the filtering quality.

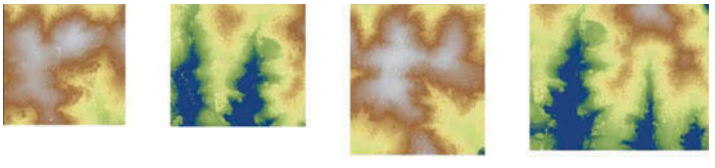

(*a*) (*b*) (*c*) (*d*)

Figure 12. Small examples of Test-site I: (*a*) Sample 11; (*b*) Sample 12; (*c*) Sample 13; (*d*) Sample 14.

Table 3. The performance of multi-features.

		With multi-features		
Data	No. points	Filtered non-terrain points	Kappa (%)	Without multi-features kappa (%)
Sample 11	185,467	27,031	0.8012	0.7924
Sample 12	214,289	30,257	0.7912	0.7784
Sample 13	301,498	40,159	0.8327	0.8213
Sample 14	357,497	56,377	0.7932	0.7845

Table 4. Effect of the number of CSPs on filtering accuracy.

Test no.	Number of CSPs ($0° \leq \varphi < 180°$)	Merge	Intersect
1	1 ($\Delta\varphi = 0°$)	0.6934	0.6934
2	2 ($\Delta\varphi = 90°$)	0.7202	0.7341
3	3 ($\Delta\varphi = 60°$)	0.7411	0.7588
4	4 ($\Delta\varphi = 45°$)	0.7929	0.8043
5	5 ($\Delta\varphi = 36°$)	0.8093	0.8134
6	6 ($\Delta\varphi = 30°$)	0.8011	0.8026
7	9 ($\Delta\varphi = 20°$)	0.8034	0.7994
8	12 ($\Delta\varphi = 15°$)	0.7755	0.7893
9	15 ($\Delta\varphi = 12°$)	0.7134	0.7446
10	18 ($\Delta\varphi = 10°$)	0.6332	0.7087

4.2.3. *Effects of the number of CSPs on filtering accuracy*

For each cell, we can generate a number of CSPs at multiple directions ranging from 0° to 180°. In this section, to assess the effect of the number of CSPs on filtering accuracy, we conduct a set of experiments by applying $\Delta\varphi$ to lidar data. For example, if $\Delta\varphi = 0°$, we project all points at only one CSP at $\varphi = 0°$; if $\Delta\varphi = 30°$, six CSPs at $\varphi = 0°$, 30°, 60°, 90°, 120°, 150°. Table 4 presents the filtering results using different numbers of CSPs. We find that kappa coefficients slightly grow with the number of CSPs increasing from one to five. Our algorithm shows a good filtering performance when $\Delta\varphi$ is between 45° and 30°, that is four or six CSPs for both merging and integrating strategies. The philosophy behind this phenomenon is that CSPs at multiple directions provide much useful information to cross-validate filtering results. However, the filtering accuracy decreases when $\Delta\varphi$ is below 30°, indicating that a smaller $\Delta\varphi$ (a larger number of CSPs) can be counterproductive. In this study, we apply four cardinal directions (0°, 45°, 90°, and 135°) to each cell of lidar data.

4.2.4. *Overall performance*

To assess the overall performance of our stepwise filtering scheme, we compare it with the progressive TIN (triangular irregular network) densification method implemented in the commercial Terrasolid® software suite. Several parameters are involved in the progressive TIN algorithm, including the maximum building size, iteration angle, and iteration distance. Although the proposed method includes six parameters listed in Table 1, only three parameters play essential roles in the classification procedure. The other parameters' thresholds are determined automatically based on the lidar point statistical characteristics: the cell size, the slope, and distance. The cell size in this study is similar to the maximum building size of the progressive TIN densification. Therefore, we keep the same values for both of them. As previously discussed, the cell size, slope, and distance thresholds are 15 m, 30º, and 1 m, respectively. We keep the same values for the maximum building size, iteration angle, and iteration distance of the progressive TIN. Figures 13(*a*) and (*b*) describe our filtering results. Figures 13(*c*) and (*d*) are filtering results represented by the progressive TIN algorithm. Note that the progressive TIN densification smooths and removes some significant terrain characteristics, while our CSP-based stepwise filtering method can better retain terrain characteristics.

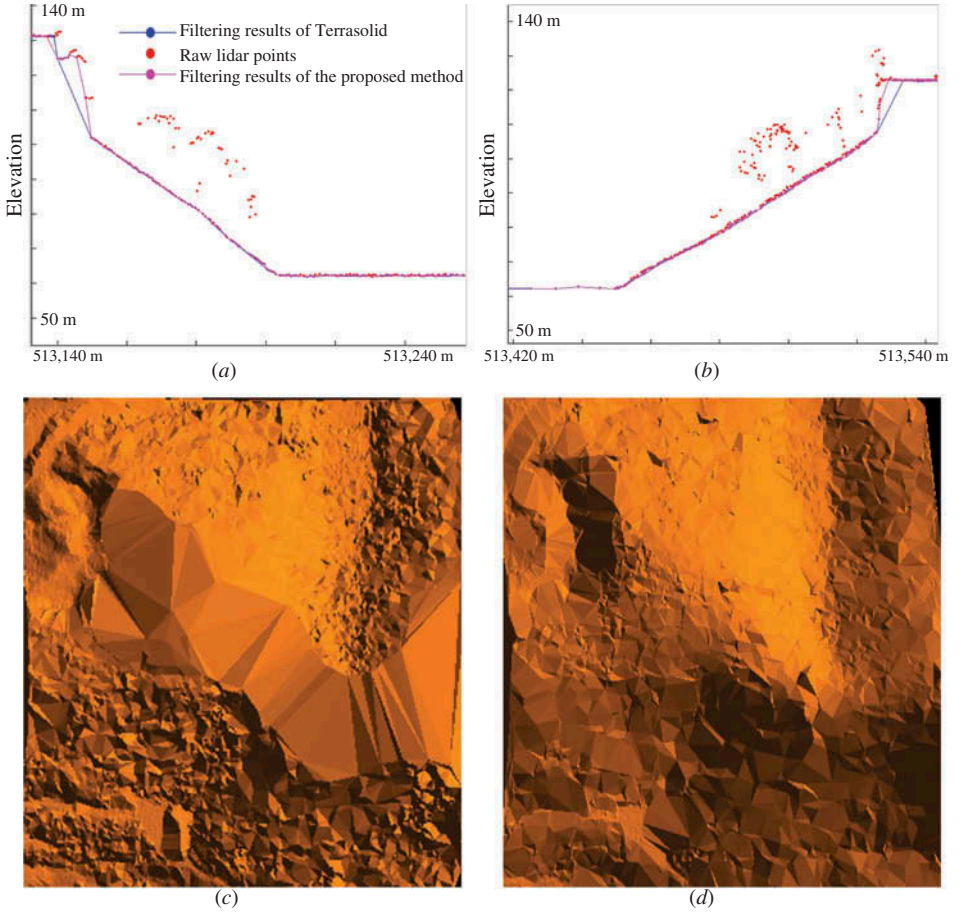

Figure 13. Comparison between progressive TIN and the proposed filtering method: (*a*) and (*b*) two filtered profiles obtained, (*c*) filtered DTM obtained by progressive TIN method and (*d*) by the proposed filtering method.

4.3. Test-site II

Figure 14 illustrates Test-site II, covering an area with dimensions of about 435 m by 426 m. The ground elevations range from 101.9 m to 228.33 m. As shown in Figure 14, the terrain changes abruptly. There are a total of 183,847 points in data set II with a density of 1 point/m^2.

Besides the error matrix with classified ground truth data, a visual inspection by constructing a TIN model manually (Meng, Currit, and Zhao 2010) is also used for accuracy assessment when ground truth data are unavailable. Figures 15(*a*) and (*b*) are filtered results of Test-site II shown from different perspectives. According to the experiment results of Test-site I, we keep thresholds of the cell size, slope, and distance as 15 m, 30°, and 1 m, respectively. A visual inspection confirms that the filtering results retain terrain features quite well, and that almost all vegetation is removed successfully. For example, ridges and valleys are still kept, though they are covered by dense vegetation, which results in an insufficient amount of ground information from poor lidar penetration.

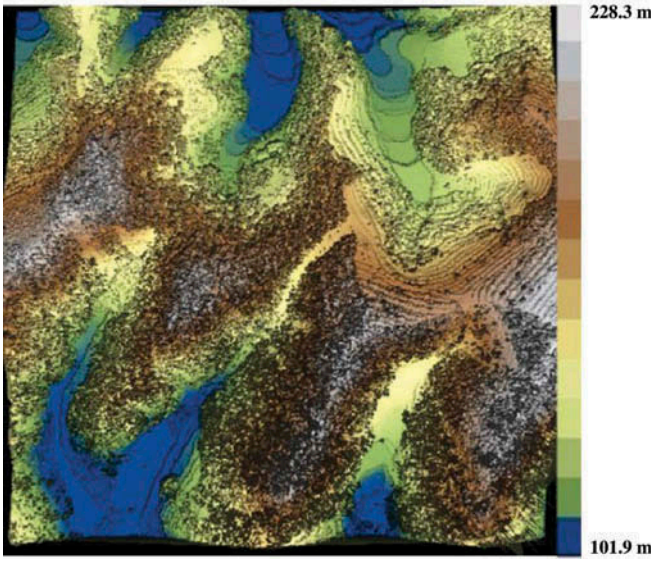

Figure 14. Test-site II.

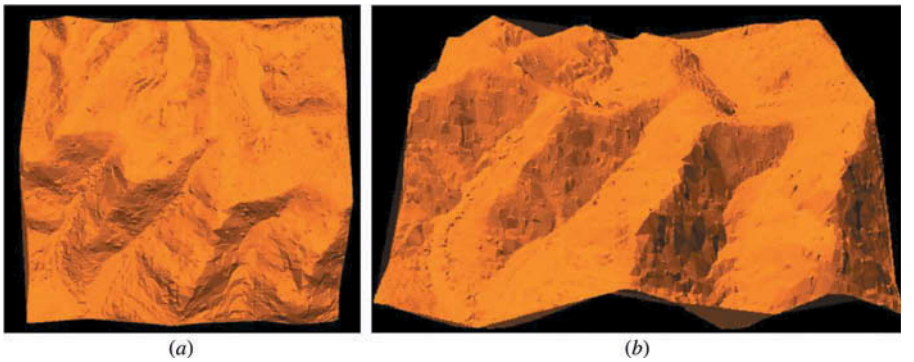

Figure 15. Illustration of filtering result of Test-site II from different views.

Our proposed filtering scheme provides a precision option for users because there are multiple filtering results for a 3D cell. Thus, users can merge or intersect the filtered results based on their requirements and point density. Figure 16 shows the intersecting and merging filtering results. As shown in Figure 16, the DTM obtained by the merging strategy is smoother than the one obtained by the intersecting strategy. Among the total of 183,847 raw points, statistics show that 43,030 points are classified as terrain points by the intersecting strategy, while 59,064 points are classified as terrain points by the merging strategy. Both strategies retain the terrain characteristics.

4.4. ISPRS data

ISPRS collected the raw lidar data using an Optech ALTM scanner, and manually generated 15 reference sites from sites 1–7 (http://www.itc.nl/isprswgiii-3/filtertest/

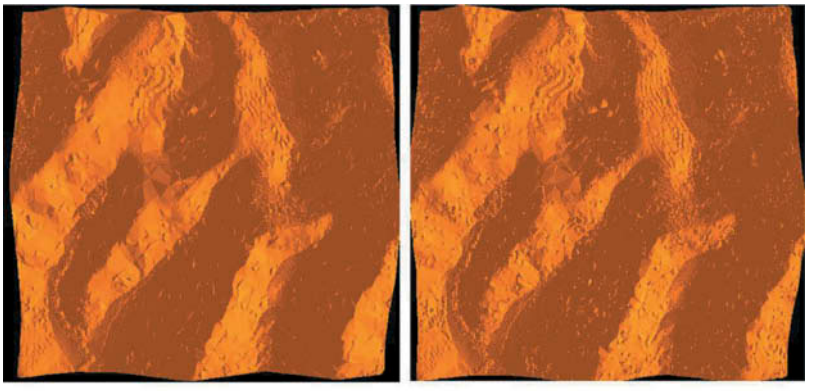

(a) (b)

Figure 16. TIN illustration of filtered results obtained by (*a*) intersecting CSPs and (*b*) merging CSPs.

index.html). A description of the characteristics of the study sites can be found in Sithole and Vosselman (2004). Sites 1–4 represent urban landscapes, while sites 5–7 represent rural landscapes (forest sites). The point density for the city and forest sites are roughly 0.67 and 0.18 points/m^2, respectively. We apply our CSP-based filtering algorithm to the 15 urban and forest study sites and calculate the ground filtering accuracy. We keep w = 15 m, $A_{\text{threshold}}$ = 20°, and $D_{\text{threshold}}$ = 1 m for city sites 1–4, which are fairly flat city terrain with few steep slopes. Rural sites 5–7 contain more drastic surface changes with lower point density than the city sites. We use w = 20 m, $A_{\text{threshold}}$ = 45°, $D_{\text{threshold}}$ = 1.5 m, and $\Delta\varphi$ = 45° (that is, four CSPs). Figure 17 shows the comparative filtering results with eight other published ground filtering methods that were tested by ISPRS on the same data sets. The average kappa coefficients of our filtering algorithm are 0.6243 and 0.7886 for city and forest sites, respectively. Compared to the performance of eight other algorithms, the CSP-based filtering algorithm generates promising results for forest test sites – it is the second best performing algorithm, although it achieves an unsatisfactory filtering performance for urban areas. Figure 17(*b*) shows that the kappa values for the CSP-based algorithm and the other three filtering algorithms (e.g. Elmqvist, Axelsson, and Pfeifer) on each site. Large and irregularly shaped buildings, or some buildings with eccentric roofs on the ground surface are a major problem for ground filtering, which causes a dramatic drop in kappa value in samples 21–24. The proposed CSP-based algorithm is capable of capturing the main ground terrain for forest sites where vegetation and buildings along steep slopes, such as samples 51 and 52, are a major challenge for most of the aforementioned filtering algorithms.

5. Conclusions

As one of the important issues in lidar applications (e.g. automatic DTM generation and feature identification), many ground filtering methods been have developed to tackle the difficulties of separating terrain from non-terrain points. However, the problem has not been fully addressed, especially for densely wooded areas. The CSP approaches provide a promising alternative by analysing multiple CSPs at different directions instead of directly estimating values within a neighbourhood. This enables multiple directional observations

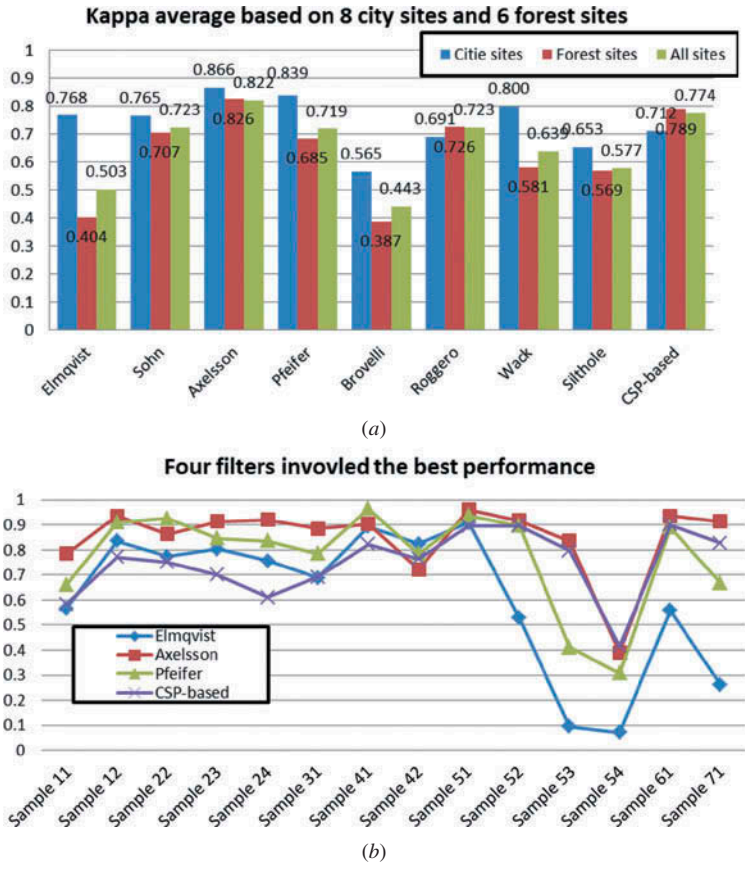

Figure 17. Kappa averages on 15 sites: (*a*) kappa values by sample site for nine filters, and (*b*) three best filters selected for comparison with our filter.

to identify more subtle surface differences in the local environment. We present a CSP-based stepwise filtering algorithm to explore the ability of a multi-directional CSP approach to use the implicit characteristics of lidar data along different directions. From a computation perspective, this approach includes four main steps: split, filter, detect, and adjust-and-refine to separate terrain from non-terrain points in wooded mountain areas.

The performance of the presented method was tested on not only two test sites covered by dense vegetation (Test-site I and Test-site II), but also an ISPRS data set including 15 study sites. In the case of Test-site I, the impact of filtering parameters on the quality of DTM has been analysed. Results show that the filtering performance is sensitive to the cell size. Specifically, the filtering accuracy decreases with the increase of the cell size. However, in densely vegetated areas, the cell size might be enlarged because the majority of lidar points are reflected from the upper canopy of vegetation rather than from the ground. Comparative experiments with the progressive TIN densification demonstrate that our method is capable of preserving more terrain features. The results of Test-site II also confirm that the CSP-based stepwise filtering method handles the lidar point cloud well in steep, densely vegetated areas. The test on ISPRS data demonstrates that our algorithm generates promising results for forest test sites by comparing the results to eight other filtering algorithms using kappa coefficients.

Our future work intends to further extend this approach and validate it with more real point cloud data sets, focusing on the following two aspects: (a) developing the algorithm so as to be threshold-free and independent from both lidar data format and point density, (b) efficiently dealing with lidar data in urban areas by dividing the space of the object into dynamic sizes to detect large and irregularly shaped buildings.

Acknowledgements

The authors wish to thank the anonymous reviewers for their insightful comments that improved the manuscript.

Funding

The research was funded in part by a discovery grant from the Natural Sciences and Engineering Research Council (NSERC) of Canada and a general grant from the National Natural Science Foundation of China (NSFC) [grant number 41071257].

References

Axelsson, P. 1999. "Processing of Laser Scanner Data – Algorithms and Applications." *ISPRS Journal of Photogrammetry and Remote Sensing* 54 (2–3): 138–147.

Axelsson, P. 2000. "DEM Generation from Laser Scanner Data Using Adaptive TIN Models." *International Archives of Photogrammetry and Remote Sensing* 33 (B4/1): 110–117.

Bartels, M., and H. Wei. 2010. "Threshold-Free Object and Ground Point Separation in Lidar Data." *Pattern Recognition Letters* 31 (10): 1089–1099.

Brenner, C. 2000. "Towards Fully Automatic Generation of City Models." *The International Archives of the Photogrammetry, Remote Sensing and Spatial Information Sciences* 33: 85–92.

Bretar, F., and N. Chehata. 2010. "Terrain Modeling from Lidar Range Data in Natural Landscapes: A Predictive and Bayesian Framework." *IEEE Transactions on Geoscience and Remote Sensing* 48 (3): 1568–1578.

Briese, C. 2010. "Extraction of Digital Terrain Models." In *Airborne and Terrestrial Laser Scanning*, edited by G. Vosselman, and H. Maas, 135–168. Dunbeath: Whittles.

Chen, Q., P. Gong, D. D. Baldocchi, and G. Xie. 2007. "Filtering Airborne Laser Scanning Data with Morphological Methods." *Photogrammetric Engineering and Remote Sensing* 73: 171–181.

Congalton, R., and R. Mead. 1983. "A Quantitative Method to Test for Consistency and Correctness of Photointerpretation." *Photogrammetric Engineering and Remote Sensing* 49 (1): 69–74.

Donoghue, D. N. M., P. J. Watt, N. J. Cox, and J. Wilson. 2007. "Remote Sensing of Species Mixtures in Conifer Plantations Using LiDAR Height and Intensity Data." *Remote Sensing of Environment* 110 (4): 509–522.

Filin, S., and N. Pfeifer. 2006. "Segmentation of Airborne Laser Scanning Data Using a Slope Adaptive Neighbourhood." *ISPRS Journal of Photogrammetry and Remote Sensing* 60: 71–80.

Habib, A. F., Y. Chang, and D. C. Lee. 2009. "Occlusion-Based Methodology for the Classification of Lidar Data." *Photogrammetric Engineering & Remote Sensing* 75 (6): 703–712.

Hyyppä, J., U. Pyysalo, H. Hyyppä, and A. Samberg. 2000. "Elevation Accuracy of Laser Scanning-Derived Digital Terrain and Target Models Forest Environment." Proceedings of the 20th EARSeL Symposium and Workshops, Lidar Remote Sensing of Land and Sea, Dresden, June 14–16, 139–147.

Kilian, J., N. Haala, and N. Englich. 1996. "Capture and Evaluation of Airborne Laser Scanner Data." *International Archive of Photogrammetry and Remote Sensing* 31 (B3): 383–388.

Kobler, A., N. Pfeifer, P. Ogrinc, L. Todorovski, K. Osti, and S. Dzeroski. 2007. "Repetitive Interpolation: A Robust Algorithm for DTM Generation from Aerial Laser Scanner Data in Forested Terrain." *Remote Sensing of Environment* 108: 9–23.

Kraus, K., and N. Pfeifer. 1998. "Determination of Terrain Models in Wooded Areas with Airborne Laser Scanner Data." *ISPRS Journal of Photogrammetry and Remote Sensing* 53: 193–203.

Li, J., and H. Guan. 2010. 3D Building Reconstruction from Lidar Point Clouds Fused with Aerial Imagery. In *Urban Remote Sensing: Monitoring, Synthesis and Modeling in the Urban Environment*, edited by X. Yang, 75–92. Chichester: Wiley-Blackwell.

Liu, X. 2008. "Airborne LiDAR for DEM Generation: Some Critical Issues." *Progress in Physical Geography* 32 (1): 31–49.

Lodha, S., E. J. Kreps, D. Helmbold, and D. Fitzpatrick. 2006. "Aerial Lidar Data Classification Using Support Vector Machines (SVM)." In *Proceedings of the Third International Symposium on 3D Data Processing, Visualization, and Transmission(3DPVT'06)*, June 14–16, 567–574. Chapel Hill, NC: IEEE.

Lu, W.-L., K. P. Murphy, J. J. Little, A. Sheffer, and H. Fu. 2009. "A Hybrid Conditional Random Field for Estimating the Underlying Ground Surface from Airborne LiDAR Data." *IEEE Transactions on Geoscience and Remote Sensing* 47 (8): 2913–2922.

Meng, X. L., N. Currit, and K. Zhao. 2010. "Ground Filtering Algorithms for Airborne Lidar Data: A Review of Critical Issues." *Remote Sensing* 2: 833–860.

Meng, X. L., L. Wang, J. L. Silván-Cárdenas, and N. Currit. 2009. "A Multi-Directional Ground Filtering Algorithm for Airborne LiDAR." *ISPRS Journal of Photogrammetry and Remote Sensing* 64: 117–124.

Mongus, D., and B. Zalik. 2012. "Parameter-Free Ground Filtering of LiDAR Data for Automatic DTM Generation." *ISPRS Journal of Photogrammetry and Remote Sensing* 67: 1–12.

Nardinocchi, C., G. Forlani, and P. Zingaretti. 2003. "Classification and Filtering of Laser Data." *The International Archives of the Photogrammetry, Remote Sensing and Spatial Information Sciences*, Dresden, October 8–10, 8 p.

Pfeifer, N., and C. Briese. 2007. "Geometrical Aspects of Airborne Laser Scanning and Terrestrial Laser Scanning." *The International Archives of the Photogrammetry, Remote Sensing and Spatial Information Sciences* 36 (part 3/W52): 311–319. http://www.ipf.tuwien.ac.at/np/Publications/Pfeifer_2007_keynote.pdf

Pfeifer, N., and G. Mandlburger. 2008. "Lidar Data Filtering and DTM Generation." In *Topographic Laser Scanning and Imaging: Principles and Processing*, edited by J. Shan, and C. K. Toth, 308–333. Boca Raton, FL: CSC Press; Taylor & Francis Group.

Pfeifer, N., T. Reiter, C. Briese, and W. Rieger. 1999. "Interpolation of High Quality Ground Models from Laser Scanner Data in Forested Areas." *International Archives of Photogrammetry and Remote Sensing* 32 (3/W14): 31–36.

Pfeifer, N., P. Stadler, and C. Briese. 2001. "Derivation of Digital Terrain Models in the SCOP++ Environment." Proceedings of OEEPE Workshop on Airborne Laser Scanning and Interferometric SAR for Detailed Digital Elevation Models, Stockholm, March 1–3, 13 p.

Raber, G. T., J. R. Jeansen, S. R. Schill, and K. Schuckman. 2002. "Creation of Digital Terrain Models Using an Adaptive Lidar Vegetation Point Removal Process." *Photogrammetric Engineering and Remote Sensing* 68 (12): 1307–1306.

Roggero, M. 2001. "Airborne Laser Scanning: Clustering Raw Data." *International Archives of Photogrammetry and Remote Sensing and Spatial Information Sciences* 34 (3/W4): 227–232.

Rosenfield, G. H., and K. Fitzpatrick-Lins. 1986. "A Coefficient of Agreement as a Measure of Thematic Classification Accuracy." *Photogrammetric Engineering and Remote Sensing* 52 (2): 223–227.

Seo, S., and C. G. O'Hara. 2008. "Parametric Investigation of the Performance of Lidar Filters Using Different Surface Contexts." *Photogrammetric Engineering & Remote Sensing* 74 (3): 343–362.

Shan, J., and A. Sampath. 2005. "Urban DEM Generation from Raw Lidar Data: A Labeling Algorithm and Its Performance." *Photogrammetric Engineering & Remote Sensing* 71 (2): 217–226.

Shao, Y., and L. Chen. 2008. "Automated Searching of Ground Points from Airborne Lidar Data Using a Climbing and Sliding Method." *Photogrammetric Engineering & Remote Sensing* 74 (5): 625–635.

Sithole, G. 2001. "Filtering of Laser Altimetry Data Using a Slope Adaptive Filter." *International Archives of Photogrammetry and Remote Sensing and Spatial Information Sciences* 34 (3/W4): 203–210.

Sithole, G., and G. Vosselman. 2004. "Experimental Comparison of Filtering Algorithms for Bare-Earth Extraction from Airborne Laser Scanning Point Clouds." *ISPRS Journal of Photogrammetry and Remote Sensing* 59: 85–101.

Sithole, G., and G. Vosselman. 2005. "Filtering of Airborne Laser Scanner Data Based on Segmented Point Clouds." *International Archives of Photogrammetry, Remote Sensing and Spatial Information Sciences* 36 (3/W3): 66–71.

Sohn, G., and I. Dowman. 2002. "Terrain Surface Reconstruction by the Use of Tetrahedron Model with the MDL Criterion." *International Archives of Photogrammetry, Remote Sensing and Spatial Information Sciences* 34 (3A): 336–344.

Tovari, D., and N. Pfeifer. 2005. "Segmentation Based Robust Interpolation – A New Approach to Data Filtering." *International Archives of Photogrammetry, Remote Sensing and Spatial Information Sciences* 36 (3/W3): 79–84.

Vosselman, G. 2000. "Slope Based Filtering of Laser Altimetry Data." *International Archives of Photogrammetry, Remote Sensing and Spatial Information Sciences* 33 (B3): 935–942.

Vosselman, G., and H.-G. Maas. 2001. "Adjustment and Filtering of Raw Laser Altimetry Data." Proceedings of OEEPE Workshop on Airborne Laser Scanning and Interferometric SAR for Detailed Digital Elevation Models, Stockholm, March 1–3, 62–72.

Wack, R., and A. Wimmer. 2002. "Digital Terrain Models from Airborne Laser Scanner Data – A Grid Based Approach." *International Archives of Photogrammetry, Remote Sensing and Spatial Information Sciences* 34 (3B): 293–296.

Wang, C., and N. F. Glenn. 2009. "Integrating LiDAR Intensity and Elevation Data for Terrain Characterization in a Forested Area." *IEEE Geoscience and Remote Sensing Letters* 6 (3): 463–466.

Zhang, K., and D. Whitman. 2005. "Comparison of Three Algorithms for Filtering Airborne Lidar Data." *Photogrammetric Engineering and Remote Sensing* 71 (3): 313–324.

Zhang, K. Q., S. C. Chen, D. Whitman, M. L. Shyu, J. H. Yan, and C. C. Zhang. 2003. "A Progressive Morphological Filter for Removing Nonground Measurements from Airborne Lidar Data." *IEEE Transactions on Geoscience and Remote Sensing* 41: 872–882.

Zhou, W., and A. Troy. 2008. "An Object-Oriented Approach for Analysing and Characterizing Urban Landscape at the Parcel Level." *International Journal of Remote Sensing* 29 (11): 3119–3135.